Guiding polarizable particles in multihole Gaussian beams

Tomasz Radożycki *

Faculty of Mathematics and Natural Sciences, College of Sciences, Institute of Physical Sciences, Cardinal Stefan Wyszyński University, Wóycickiego 1/3, 01-938 Warsaw, Poland

(Received 5 April 2024; revised 30 May 2024; accepted 18 July 2024; published 16 August 2024)

The present paper discusses the application of certain special Gaussian beams that, thanks to some polynomial prefactors, have uniquely designed holes in the irradiance. Such holes, or rather tubes, can constitute potential valleys for negatively polarizable particles, providing the possibility of guiding several objects of that kind, each along its own trajectory. The mechanism of creating these holes by interference of Gaussian beams which exhibit orbital angular momentum is discussed, and then the trajectories of particles moving in such a wave are numerically calculated. As it turns out, these particles, performing transverse oscillations, follow the designed tunnels of low irradiance. On the contrary, for particles with positive polarizability these areas are inaccessible.

DOI: 10.1103/PhysRevA.110.023515

I. INTRODUCTION

As is well known, if polarization effects do not play a significant role, a laser beam near the propagation axis can be effectively described by the simplified scalar Helmholtz equation. The approximation is accomplished by substituting into the wave equation

$$\left(\triangle_\perp + \partial_z^2 - \frac{1}{c^2}\,\partial_t^2\right)\Psi(\boldsymbol{r}, z, t) = 0, \tag{1}$$

where $\triangle_\perp$ denotes the transverse two-dimensional Laplace operator, the solution in the form

$$\Psi(\boldsymbol{r}, z, t) = e^{ik(z-ct)}\psi(\boldsymbol{r}, z), \tag{2}$$

where $\psi(\boldsymbol{r}, z)$ is assumed to be a slowly varying function of the coordinate z. The electric field is then related to $\Psi(\boldsymbol{r}, z, t)$ in the standard way:

$$\boldsymbol{E}(\boldsymbol{r}, z, t) = \boldsymbol{E}_0\Psi(\boldsymbol{r}, z, t) \tag{3}$$

with $\boldsymbol{E}_0$ representing a constant vector [upon satisfying the condition $\boldsymbol{E}_0 \cdot \nabla\Psi(\boldsymbol{r}, z, t) \approx 0$]. The bold symbol $\boldsymbol{r}$ (and later $\boldsymbol{\xi}$) denotes the two-dimensional vector lying in the plane perpendicular to the direction of propagation, e.g., $\boldsymbol{r} = [x, y]$.

Upon neglecting the second-order derivative with respect to z due to

$$\left|\partial_z^2\psi\right| \ll |k\partial_z\psi|, \tag{4}$$

where ∂_z denotes ∂/∂_z, one gets the so-called *paraxial equation* for the scalar envelope $\psi(\boldsymbol{r}, z)$ [1]:

$$(\triangle_\perp + 2ik\partial_z)\psi(\boldsymbol{r}, z) = 0. \tag{5}$$

This approximation was worked out in detail by Lax and collaborators [2].

The fundamental solution to this equation, called the Gaussian beam (GB), has been known since 1966 (see [3]) and has been extensively investigated within, but also beyond, the validity of the paraxial approximation (see, for instance, [1,4–11]).

The principal feature of the GB, contrary to the unphysical and idealized infinite plane waves, constitutes the inhomogeneity in the distribution of the wave intensity, especially the presence of a narrowing, termed the beam waist, where the concentration of energy is maximal. This property enabled the trapping of neutral polarizable particles and the design of the so-called optical tweezers, i.e., gradient force traps [12–15].

The structure of the GB is further enriched if it is endowed with nonzero orbital angular momentum (OAM). In this case, the beam has a vortical nature: on its axis the irradiance drops to zero, and upon encircling it the phase changes by $2\pi n$, where $n\hbar$ denotes the value of the OAM. Such beams can be said to be "hollow" along the propagation axis. The surfaces of the constant phase are then of helical character.

The original optical tweezers operated due to gradient forces pulling particles of positive polarizability into areas of high wave intensity. In a similar way, the irradiance "holes" can serve as traps or guidelines for objects of negative polarizability such as atoms in blue-detuned beams [16–18]. The identical effect is due to the ponderomotive force acting on charged particles, such as electrons, originating from the inhomogeneous circularly polarized wave [19,20].

As a recent experimental example of the use of so-called dark focus tweezers one can refer to Ref. [21], which demonstrates trapping of nanometer-sized silicon balls placed in an external medium to achieve a relative refractive index less than 1. A hollow beam called a "bottle beam" [22] was obtained in this study by superposition of Gaussian and Laguerre-Gaussian beams. Numerous references to other theoretical and experimental findings can be found in the works cited above.

Dark focus tweezers or hollow beams have the advantage that particles are trapped or guided in the low-radiation

*Contact author: t.radozycki@uksw.edu.pl

 ©2024 American Physical Society

domain and are therefore less likely to be damaged. This is particularly significant for biological objects.

In this paper, we focus on certain hollow Gaussian beams which represent the solutions to the paraxial equation and which can be designed to suit specific purposes, such as guiding several particles or atoms in a special way. For years hollow beams have been of interest to researchers due to their possible applications in particle trapping and also in atomic physics or optical communication (see, for instance, [23–27]). As mentioned above, however, typically, this term refers to the situation in which light is concentrated outward on a cylindrical or annular structure with a hollow space in the center aligned along the propagation axis (certain non-cylindrical hollow beams of elliptical or rectangular cross section were introduced in [26]). To this category belong not only the well-known Bessel-Gaussian and Laguerre-Gaussian beams but also other ones (see, for instance, [1,11,17,28–37]). In contrast, the beams dealt with in the present work are generated as superpositions of two or more coaxial Gaussian modes with specific OAM values, which lead to the development of a *multihole* structure. Naturally, a superposition of cylindrical waves with different angular momenta is no longer a cylindrical beam in the sense that the distribution of the irradiance does not exhibit axial symmetry. Depending on the choice of the constituent modes, this multitube (i.e., multihole) structure can be designed as needed. This issue will be discussed in detail in the next section.

This type of beam has been known in the literature for about 30 years, although apparently not in the context of guiding particles. To mention just a few results one can first refer to Ref. [38], which, after a rather general introduction containing theoretical foundations of the so-called arrays of vortices, provides numerical results concerning vortex-vortex and vortex-antivortex interactions. In turn the experimental work in Ref. [39] demonstrated the generation of a two-hole beam thanks to the diffraction on the computer-synthesized grating and examined the stability of closely located vortices. In [40] the authors focused on the numerical analysis of the motion and interaction of vortices inserted in a Gaussian beam in linear and nonlinear media.

This kind of structured light is expected to find potential application in communication. For this reason, the stability of hollow beams subjected to random phase distortions has also been investigated [41].

In Sec. III the possible use of this structure to transport particles in a certain way will be addressed. For example, a multihole beam can simultaneously guide several particles, each in its own potential tube. This paper is concerned with a theoretical qualitative, rather than quantitative, description of this phenomenon.

Among all the research areas mentioned above, the manipulation of particles still remains a key problem because of its wide potential usage in physics, chemistry, biology, and medicine (see, for instance, [15,42–47]) and constitutes one of the major applications of structured light. In particular, apart from three-dimensional traps, guiding particles by light along predesigned trajectories, as in [48–50], continues to be an exciting topic, and both purely theoretical and experimental research in this area seems to be of importance.

II. DESCRIPTION OF MULTIHOLE GAUSSIAN BEAMS

Before proceeding, it is convenient to introduce dimensionless coordinates according to the formulas

$$\xi_x = \frac{x}{w_0}, \quad \xi_y = \frac{y}{w_0}, \quad \zeta = \frac{z}{z_R}, \tag{6}$$

where w_0 is the beam waist and $z_R = \frac{kw_0^2}{2}$ denotes the Rayleigh length, i.e., the distance at which the area of the transverse section of the beam increases twice. A different designation is used for the transverse components ξ_x and ξ_y and for the longitudinal component ζ, as they play a somewhat different role in the subsequent expressions. With this notation the paraxial equation (5) takes the following form:

$$(\triangle_{\xi\perp} + 4i\partial_\zeta)\psi(\boldsymbol{\xi}, \zeta) = 0, \tag{7}$$

where $\boldsymbol{\xi} = [\xi_x, \xi_y]$. The solution can be looked for in the following form:

$$\psi(\boldsymbol{\xi}, \zeta) = \frac{1}{1+i\zeta} e^{-\frac{\xi^2}{1+i\zeta}}\, \tilde{\psi}(\boldsymbol{\xi}, \zeta). \tag{8}$$

After the substitution of (8) into (7), one can easily derive the differential equation for the unknown function $\tilde{\psi}(\boldsymbol{\xi}, \zeta)$:

$$\xi\, \partial_\xi \tilde{\psi}(\xi, \zeta) = i(1+i\zeta)\partial_\zeta \tilde{\psi}(\xi, \zeta), \tag{9}$$

which is satisfied by any function of one combined argument $\frac{\xi}{1+i\zeta}$, i.e.,

$$\tilde{\psi} = \tilde{\psi}\left(\frac{\xi}{1+i\zeta}\right). \tag{10}$$

In formulas (9) and (10) the complex coordinate $\xi = \xi_x + i\xi_y$ is introduced and should be distinguished from $|\boldsymbol{\xi}| = \sqrt{\xi_x^2 + \xi_y^2} = |\xi|$. Result (10) is well known [51]. In particular the choice of $\tilde{\psi}(s) = \text{const}$ leads to the fundamental GB, and $\tilde{\psi}(s) = \text{const} \times s^n$ corresponds to the GB of vorticity n.

Let us now concentrate on the zeros of the envelope ψ. From formula (8) it is obvious that it does not have any zeros other than those of the function $\tilde{\psi}$. Let $p = p_r + ip_i = p_0 e^{i\phi_0}$ be any of them. As ζ increases, i.e., when moving upward along the beam, the radial distance of this zero from the beam axis grows, which is consistent with the diffraction of the beam itself, but its position also gets twisted around it by an angle asymptotically tending to $\pi/2$, as indicated in the formulas

$$|\boldsymbol{\xi}| = \frac{p_0}{\beta}\sqrt{1+\zeta^2},$$
$$\phi(\zeta) = \phi_0 + \arctan\zeta, \tag{11}$$

where β is a certain constant playing the role of the scaling factor defined below in (12). Since all possible zeros follow synchronized identical paths, they never merge, their number remains constant along the beam, and each develops its own nodal line as the value of ζ increases (naturally in the opposite direction, i.e., for $\zeta < 0$ as well). This effect was observed in [38].

The simplest function that can be picked is a polynomial, which corresponds to the interference of a couple of coaxial Gaussian beams with differing OAM values. Of course, $\tilde{\psi}$ is at our disposal, and any analytic function could play

this role, although a nonpolynomial function would require a superposition of infinitely many modes (from the practical point of view, however, low-intensity high-order beams might be ignored). For the purposes of this paper, the function $\tilde{\psi}$ is chosen in the form of a particularly simple polynomial:

$$\tilde{\psi}(s) = (\beta s)^n - 1. \tag{12}$$

The scaling role of the parameter β has already been mentioned and is clear in (12). This form indicates that the interference of exactly two Gaussian beams is dealt with: one of order 0,

$$\psi_0(\boldsymbol{\xi}, \zeta) = \frac{1}{1 + i\zeta} e^{-\frac{\xi^2}{1+i\zeta}}, \tag{13}$$

and one of order n:

$$\psi_n(\boldsymbol{\xi}, \zeta) = \frac{\beta^n \xi^n}{(1 + i\zeta)^{n+1}} e^{-\frac{\xi^2}{1+i\zeta}}. \tag{14}$$

In our analysis the overall normalization constants are omitted, as only relative beam intensities are essential (in a sense represented by the value of the parameter β).

Beam (12) bears the vortex topological charge n, and when encircling the axis ζ the value of the phase increases by $2\pi n$, which means that it assumes n times the same values (if reduced to the interval $[0, 2\pi[$). Thus, on a circle (for $\zeta = \text{const}$) of radius $\sqrt{1 + \zeta^2}/\beta$ (in units of w_0) a completely destructive interference with $\tilde{\psi}_0$ occurs exactly n times. The nth degree vortex "spreads" into n individual vortices (in the case of Bessel beams the same phenomenon was demonstrated in [52]), uniformly distributed, as is obvious from the distribution of the nth complex roots of the unity. Consequently, n holes in the wave intensity appear in the perpendicular plane, as shown in Fig. 1 for $n = 3$. In Figs. 1(a)–1(h), which have increasing values of ζ, the diffraction of the wave and the twisting of the whole pattern can be seen, in agreement with (11).

In Fig. 2 the irradiance of the same beam in four axial planes is drawn. The first plane is simply the $\xi_x\zeta$ plane, and the subsequent ones are rotated around the ζ axis by successive multiples of $\pi/10$. The formation of the zero-intensity tubes is marked with arrows.

Figures 3 and 4 demonstrate the same effects for $n = 5$. The existence of five distinct roots of unity yields five "tubes" of vanishing irradiance that can eventually be exploited. A slightly reduced value for the parameter β has been chosen in this case in order to avoid merging areas of low energy density.

Naturally, in the role of $\tilde{\psi}$ other polynomials that would not have zeros distributed in such a regular fashion come into play as well.

In order to visualize the splitting of one vortex of higher topological charge into several single ones it is convenient to analyze the phase of the beam in the perpendicular planes. Fully destructive interference requires (apart from the equality of the wave amplitudes) the phases of the two interfering waves at a given point to differ by an odd multiple of π. It is known that at such places, the overall phase ϕ of the combined wave becomes indeterminate.

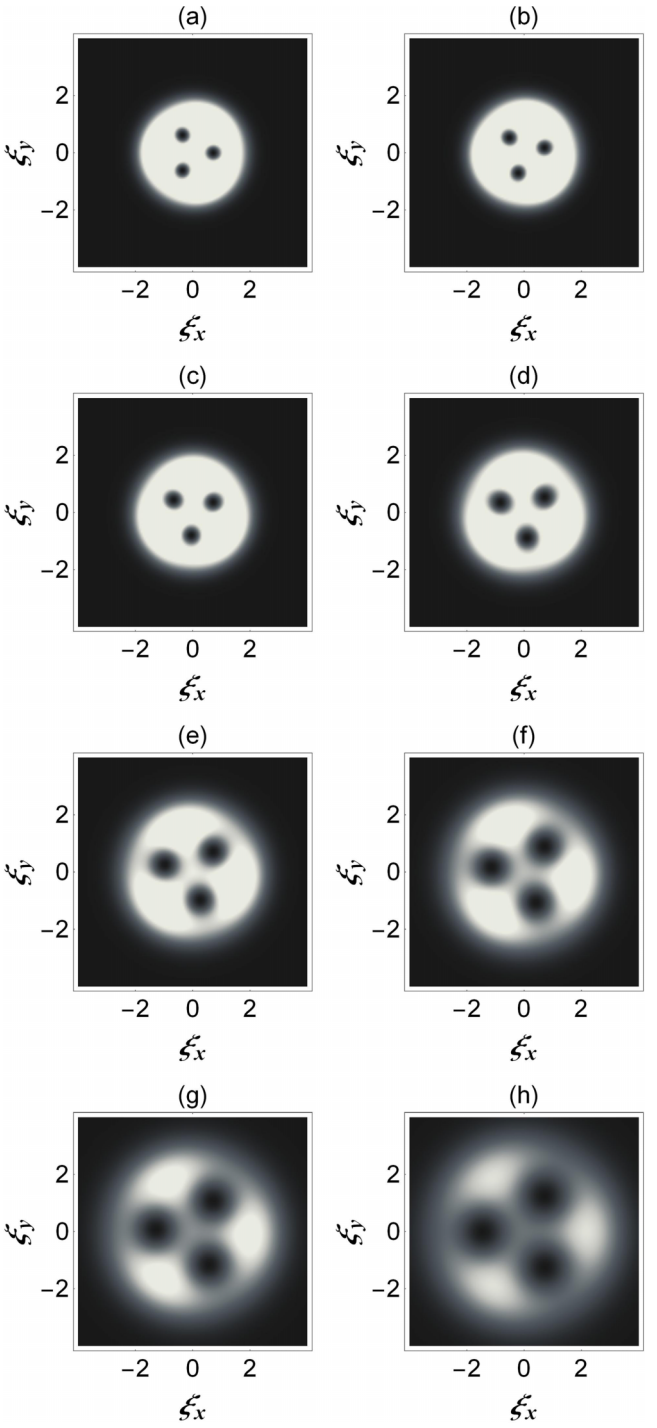

FIG. 1. The irradiance, in the perpendicular plane, of the beam created as the plain superposition of (13) and (14) for $n = 3$ according to (12). The following values of ζ are used: (a) 0, (b) 0.25, (c) 0.5, (d) 0.75, (e) 1, (f) 1.25, (g) 1.5, and (h) 1.75. The parameter $\beta = 1.4$. Bright areas represent high irradiance, and dark ones represent low irradiance.

The change in phase along a certain closed curve $\mathcal{C}$ is defined by the formula

$$\Delta_{\mathcal{C}}\phi = \oint_{\mathcal{C}} \nabla\phi \, d\boldsymbol{l} = -\frac{i}{2} \oint_{\mathcal{C}} \frac{\Psi^* \overleftrightarrow{\nabla} \Psi}{\Psi^* \Psi} \, d\boldsymbol{l}, \tag{15}$$

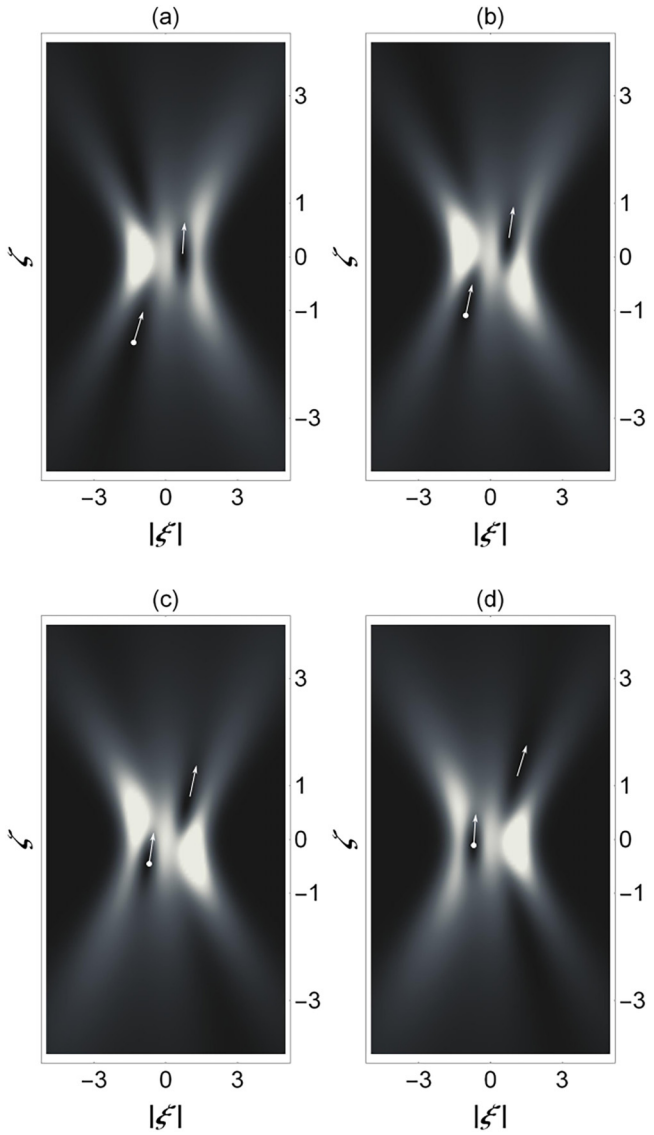

FIG. 2. Same as Fig. 1, but in the axial plane. Graphs present the view of the same beam from different angles between the x axis and the line of sight: (a) 0, (b) 0.1π, (c) 0.2π, and (d) 0.3π. The two types of white arrows mark two twisting tubes with low irradiance.

where $*$ denotes the complex conjugation. In the case dealt with here the integration contour can be deformed to a flat one lying in the plane $\zeta = \text{const}$, such as those shown by white circles in Fig. 5. Then the nabla operator reduces to two dimensions (vector $d\boldsymbol{l}$ does not have the ζ component), and $\Delta_C\phi$ can be represented in the form of the complex contour integral with respect to $d\xi = d\xi_x + id\xi_y$:

$$\begin{aligned}\Delta_C\phi &= -\frac{i}{2}\oint_C\left(\frac{\boldsymbol{\nabla}\psi}{\psi} - \frac{\boldsymbol{\nabla}\psi^*}{\psi^*}\right)d\boldsymbol{l}\\ &= -\frac{i}{2}\oint_C\left[\frac{1}{\psi}(d\xi_x\,\partial_{\xi_x}\psi + d\xi_y\,\partial_{\xi_y}\psi)\right.\\ &\quad\left. - \frac{1}{\psi^*}(d\xi_x\,\partial_{\xi_x}\psi^* + d\xi_y\,\partial_{\xi_y}\psi^*)\right]. \qquad (16)\end{aligned}$$

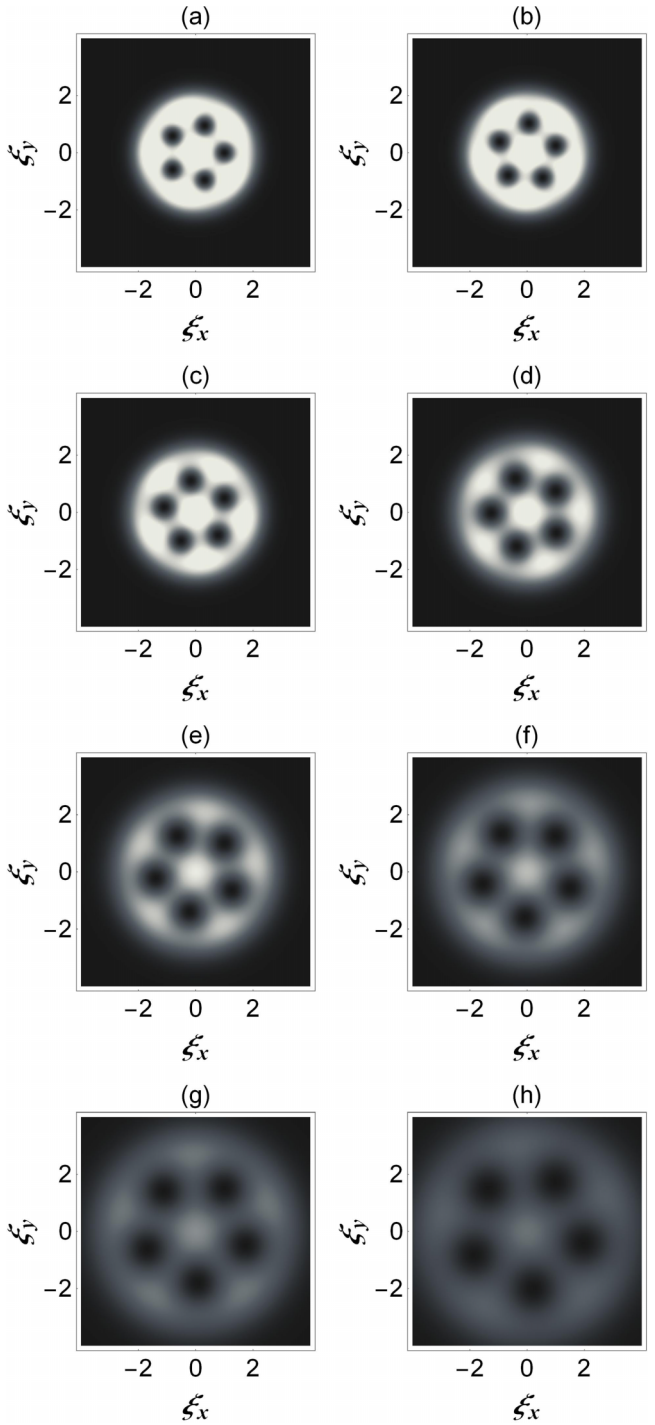

FIG. 3. Same as Fig. 1, but for $n = 5$ and $\beta = 1$.

The function ψ formally depends on two complex variables, ξ and ξ^*, so

$$\begin{aligned}\partial_{\xi_x}\psi &= (\partial_\xi + \partial_{\xi^*})\psi,\\ \partial_{\xi_y}\psi &= i(\partial_\xi - \partial_{\xi^*})\psi, \qquad (17)\end{aligned}$$

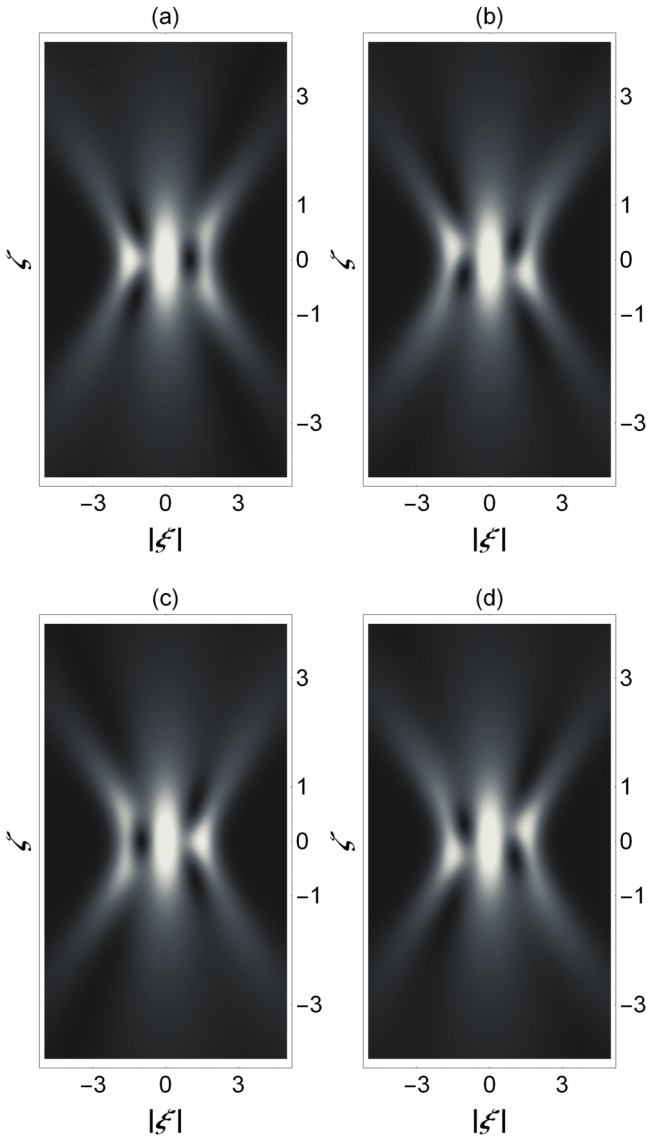

FIG. 4. Same as Fig. 2, but for $n = 5$ and $\beta = 1$.

with identical notation for ψ^*. Expression (16) may then be rewritten as

$$\Delta_C\phi = -\frac{i}{2}\oint_C \left[\frac{\partial_\xi \psi}{\psi}\,d\xi + \frac{\partial_{\xi^*}\psi}{\psi}\,d\xi^* - \frac{\partial_\xi \psi^*}{\psi^*}\,d\xi - \frac{\partial_{\xi^*}\psi^*}{\psi^*}\,d\xi^*\right]. \tag{18}$$

The value of this integral can be obtained either by direct substitution or via the Cauchy argument principle. Formally, ψ is not holomorphic in any domain because it depends on ξ^*. However, for functions ψ of the form $f(\xi)e^{-a\xi\xi^*}$, the terms in which the exponential is subject to differentiation do not contribute since

$$\oint_C (\xi^* d\xi + \xi d\xi^*) = 0. \tag{19}$$

In all other terms (i.e., those in which the exponential is not differentiated) the exponentials in the numerator and denominator cancel out, and the trace of ξ^* disappears from the expression. Therefore, from a practical point of view the function ψ may be treated as holomorphic, and that is how it is handled below. In general, this argumentation does not necessarily apply for beams for which the function f also depends on ξ^*, such as the Hermite-Gaussian beam [1,3] or that of [53].

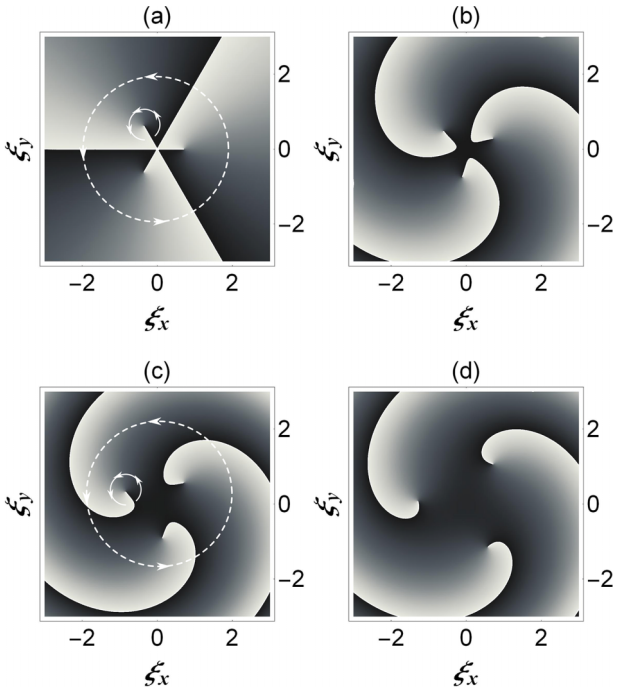

FIG. 5. The phases of the wave function of Fig. 1 depicted in four planes: (a) $\zeta = 0$, (b) 0.4, (c) 0.8, and (d) 1.5. The value of the phase, modulo 2π, is represented continuously by means of the gray scale from $-\pi$ (black) to π (white). The rotation of the entire picture with increasing ζ is due to the factor $1 + i\zeta$ in (13) and(14) and the additional factor $e^{ikz} = e^{i\zeta}$ from (2). The small white circle represents the curve $\mathcal{C}$ circulating around one of the individual vortices produced by the breakdown of the vortex with topological charge $n = 3$. The large dashed white circle encircles all the resultant vortices.

Consequently, keeping in mind (19), we can write

$$\Delta_C\phi = -\frac{i}{2}\left[\oint_C \frac{\partial_\xi \psi}{\psi}\,d\xi - \left(\oint_C \frac{\partial_\xi \psi}{\psi}\,d\xi\right)^*\right]. \tag{20}$$

The Cauchy argument principle leads to

$$\oint_C \frac{\psi'}{\psi}\,d\xi = 2\pi i(Z - P), \tag{21}$$

where Z denotes the number of zeros and P is the number of poles in the area encompassed by the curve $\mathcal{C}$. However, ψ has no poles, and the only zeros come from the polynomial (12); hence, we come to

$$\oint_C \nabla\phi\, d\boldsymbol{l} = 2\pi Z. \tag{22}$$

Since this polynomial has n single zeros, for the integral over the small white circles in Fig. 5 one always gets a value of 2π, and for the large circles one gets $2\pi n$ (here $n = 3$), which means that the total vorticity is unchanged and the vortex

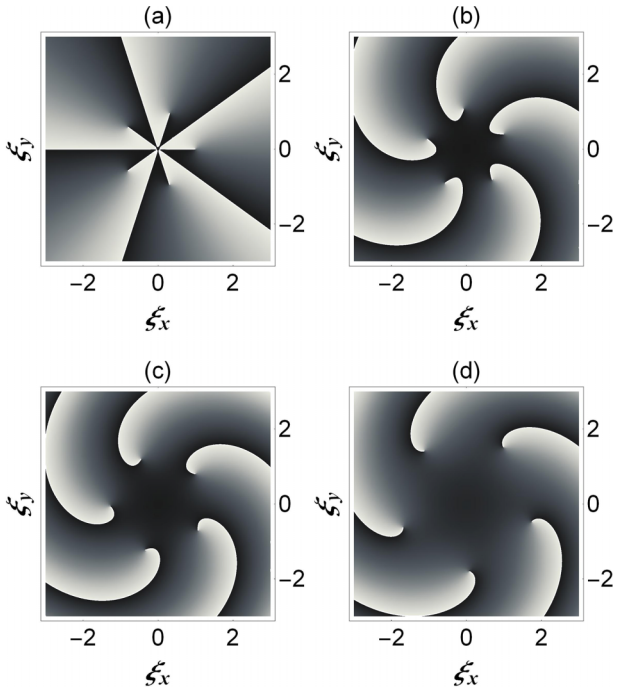

FIG. 6. Same as Fig. 5, but for $n = 5$ and $\beta = 1$.

merely gets split into n single vortices. Naturally, the same can be observed in Fig. 6.

III. GUIDING OF PARTICLES

As is well known, inhomogeneities in the intensity of the wave, and hence in the electric field, can be exploited to trap and guide neutral particles, for instance, atoms and dielectric balls, which undergo polarization in external fields. This has become the basis for the operation of the so-called optical tweezers [12–15], as mentioned in the Introduction.

Let us denote by α the particle polarizability, which, in general, can depend on the driving frequency, and by d the induced dipole moment. Then

$$\boldsymbol{d} = \alpha \boldsymbol{E}. \tag{23}$$

When speaking of atoms, from the theory of the ac Stark effect it is known that for a red-detuned beam the atomic polarizability α is positive, and for blue-detuned one it becomes negative, which affects the motion of atoms in a fundamental way. Similar conclusions can be drawn from a purely classical model of the atom [54,55]. The analogous effect in the case of dielectric nanospheres is due to the value of the refractive index being higher or lower than that of the surrounding media.

The Newton equation of motion of an atom (or other particle) in these conditions takes the form

$$m\ddot{\boldsymbol{r}} = \tfrac{1}{2}\alpha \nabla (E^2) + \boldsymbol{F}_{\text{scat}}, \tag{24}$$

where the right-hand side of the equation is treated as being averaged over the fast oscillations of the field in (2). The first term represents the conservative gradient force, and $\boldsymbol{F}_{\text{scat}}$ stands for the scattering force, which will be dealt with below in some detail.

The irradiance in this kind of beams varies rapidly in directions orthogonal to the beam axis and relatively slowly alongside it, so the perpendicular components of $\boldsymbol{F}_{\text{scat}}$ can be ignored compared to the gradient force, and only the parallel one needs to be accounted for, which is confirmed below. In order to estimate the magnitude of this force we will focus on the example of dielectric nanospheres. The influence of this force on atoms can be reduced by using a far-detuned beam, although it should be kept in mind that the gradient force is also weakened in this way.

It is known [56,57] for dielectric spheres that one has

$$\frac{F_{\text{scat}\,z}}{F_{\text{grad}\,z}} = \frac{n_s k^4 \alpha}{3\pi n_m^3 \varepsilon_0} \frac{I}{\partial_z I}, \tag{25}$$

where n_s is the refractive index of the sphere, n_m is the refractive index of the surrounding media, ε_0 is the vacuum permittivity, and I stands for the irradiance. In the dimensionless coordinates ξ_x, ξ_y, and ζ defined in (6) this ratio can be given the form

$$\frac{F_{\text{scat}\,\zeta}}{F_{\text{grad}\,\zeta}} = \frac{n_s}{n_m^3} \zeta_R \kappa \frac{I}{\partial_\zeta I}, \tag{26}$$

with $\zeta_R = k z_R$ and $\kappa = \frac{k^3 \alpha}{3\pi\varepsilon_0}$. Let us estimate these quantities for Rayleigh particles placed in a tightly focused light beam with the waist radius $w_0 = 0.05\,\text{mm}$ and wavelength $\lambda = 700\,\text{nm}$ for which $\zeta_R \approx 10^5$. In order to find the magnitude of κ one has to think of a concrete sample of particles. Take, for example, magnesium fluoride nanoballs ($n_s = 1.38$) of diameter $D = 10\,\text{nm}$ placed in glycerol ($n_m = 1.47$). In these conditions one gets $\kappa \approx -1.1 \times 10^{-5}$, where the well-known formula for the polarizability [57] has been used:

$$\alpha = \frac{1}{2} n_m^2 \varepsilon_0 D^3 \frac{n_s^2/n_m^2 - 1}{n_s^2/n_m^2 + 2}. \tag{27}$$

Consequently, the whole factor in (26) equals

$$\frac{n_s}{n_m^3} \zeta_R \kappa \approx -0.48. \tag{28}$$

In regard to the quotient $\frac{I}{\partial_\zeta I}$, it should be kept in mind that inside the tube of low irradiance, I drops to zero (together with the scattering force). Naturally, the same is true for $\partial_\zeta I$ (since the vortex core constitutes the irradiation minimum), but the latter decline is weaker, as shown below.

For the beams dealt with in this work, defined in (12), (13), and (14) the needed ratio can be calculated as

$$\left|\frac{I}{\partial_\zeta I}\right| = \left|\frac{|\Psi|^2}{\partial_\zeta |\Psi|^2}\right| = \left| -\frac{2(n+1)\zeta}{1+\zeta^2} + \frac{4|\xi|^2\zeta}{(1+\zeta^2)^2} - \sum_{l=0}^{n-1}\left(\frac{\partial_\zeta \xi_l}{\xi - \xi_l} + \frac{\partial_\zeta \xi_l^*}{\xi^* - \xi_l^*}\right)\right|^{-1}, \tag{29}$$

where

$$\xi_l = \frac{1}{\beta}(1 + i\zeta) e^{\frac{2\pi i l}{n}}, \quad \partial_z \xi_l = \frac{i}{\beta} e^{\frac{2\pi i l}{n}}. \tag{30}$$

For particles guided in the ith tube $|\xi - \xi_i| \ll 1/\beta$, and the ith term in the sum in (29) dominates over all other ones.

Therefore,

$$\frac{F_{\mathrm{scat}\,\zeta}}{F_{\mathrm{grad}\,\zeta}} \approx \frac{n}{n_s^3}\,\zeta_R\kappa \left| \frac{\xi - \xi_i}{\partial_\zeta \xi_i} + \frac{\xi^* - \xi_i^*}{\partial_\zeta \xi_i^*} \right| \ll 1, \tag{31}$$

and the scattering force should not have a relevant effect on the motion of guided particles.

This estimate was carried out for tightly focused beams. They can be broadened at the price of increasing the scattering force (it grows quadratically with w_0, provided the local energy density is maintained). However, this has no significant effect on the trajectories of guided particles (there is a quantitative effect but not a qualitative one), as tested numerically.

The scattering force has a little more significant effect for wider trajectories that depart from the core of vanishing irradiance but becomes truly essential for particles of positive polarizability which avoid areas of low irradiance. The motion of this type of particle is also shown in several figures below; therefore, $F_{\mathrm{scat}\,\zeta}$ is taken into account in all numerical calculations.

Consequently, the smoothed (with respect to time) equations of motion can be given in the following form:

$$\ddot{\xi}_x = \gamma\, \partial_{\xi_x} |\psi(\boldsymbol{\xi}, \zeta)|^2, \tag{32a}$$

$$\ddot{\xi}_y = \gamma\, \partial_{\xi_y} |\psi(\boldsymbol{\xi}, \zeta)|^2, \tag{32b}$$

$$\ddot{\zeta} = \tilde{\gamma} \left(\partial_\zeta |\psi(\boldsymbol{\xi}, \zeta)|^2 + \frac{n_s}{n_m^3}\,\zeta_R\kappa |\psi(\boldsymbol{\xi}, \zeta)|^2 \right), \tag{32c}$$

where the coefficients γ and $\tilde{\gamma}$ are expressed through the beam's parameters and particle mass,

$$\gamma = \frac{\alpha E_0^2}{4 w_0^2 \omega^2 m}, \tag{33a}$$

$$\tilde{\gamma} = \frac{\alpha E_0^2}{4 z_R^2 \omega^2 m} = \gamma \left(\frac{2}{k w_0} \right)^2 = \frac{2}{\zeta_R}\,\gamma, \tag{33b}$$

and $\omega = kc$. Depending on the sign of α, the tubes described in the preceding section constitute either some kind of potential "valley" ($\gamma < 0$) or repulsive-potential "hill" ($\gamma > 0$). Naturally, it is impossible to derive analytical solutions to the equations of motion in this kind of potential, but trajectories of particles can be found numerically for certain illustrative γ values.

Figure 7 shows, from two different perspectives, that the trajectories of three negatively polarizable particles, having been inserted into the beam shown in Figs. 1, 2, and 5, follow the irradiance holes. The value of $\gamma = 0.06$ was chosen for visualization purposes. Note the expansion of the particle's trajectory as it moves along the potential tube. It is related to the lowering of the potential barrier, which is associated with the beam's diffraction and with some acceleration of the particle. This potential barrier decreases proportionally to $1/w(z)^2$ or $1/(1+\zeta^2)$. Over a distance of one Rayleigh length it then decreases twice. The potential valley becomes shallower, and the trajectory becomes proportionally wider. From a practical point of view, such a distance seems sufficient.

The lowering of the barrier height and width may be important for the eventual hopping of particles between different potential valleys. Especially in the quantum case, it affects the tunneling probability of guided elementary particles between

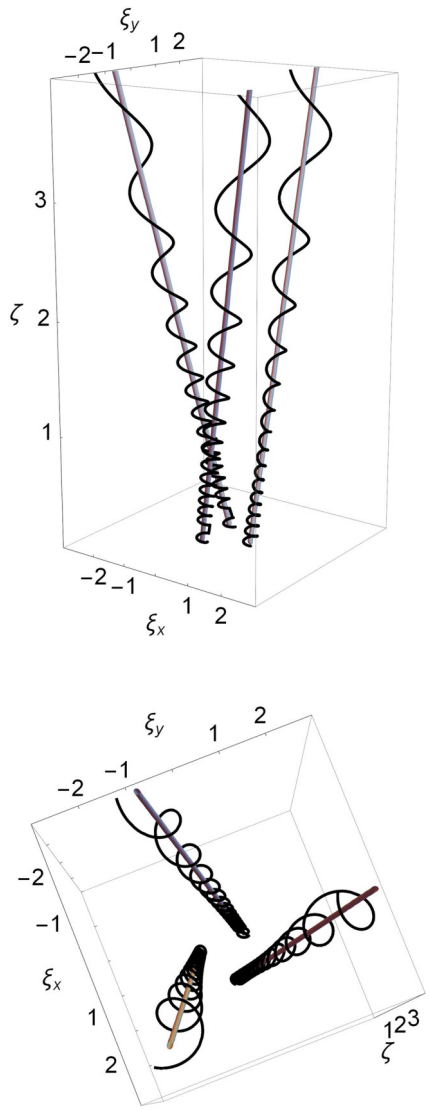

FIG. 7. The trajectories of three particles of negative polarizability placed in the "holes" of the beam in question for $n = 3$, viewed from the side and from above. Straight lines represent zero-irradiance tubes, which undergo diffraction. The values of beam parameters are the same as in Fig. 1, and $\gamma = 6 \times 10^{-2}$ and $\tilde{\gamma} = 2 \times 10^{-5}$.

various minima. Roughly speaking, if one neglects the possible acceleration of particles due to the gradient and scattering forces along the beam, the tunneling probability p increases with ζ as $p^{(1+\zeta^2)^{-1/2}}$.

Figure 8 shows the exemplary effect of the escape of one of the guided particles due to insufficient cooling and imprecise initial conditions which entail more chaotic motion. In [58] strong correlation between the chaoticness of classical trajectories of particles and the quantum tunneling probability in a trap constructed of a Bessel beam and constant magnetic field was established.

Figure 9 demonstrates the same phenomenon as Fig. 7 for five particles placed in the five-hole beam in Figs. 3, 4, and 6. For more complex beams, with a larger number of potential valleys, the issue becomes more challenging, owing to the very complicated arrangement of valleys and hills, which

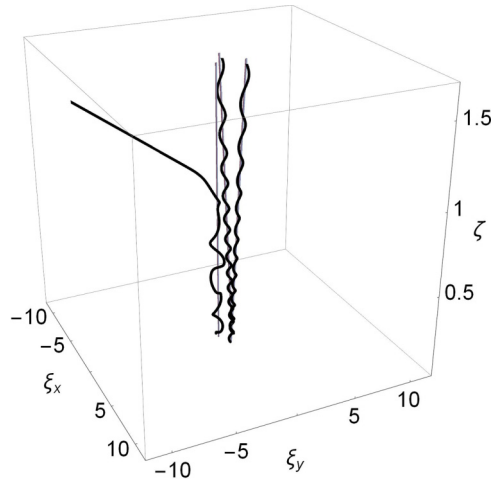

FIG. 8. Escape of a particle from the potential tube. The values of the parameters are the same as in Fig. 7.

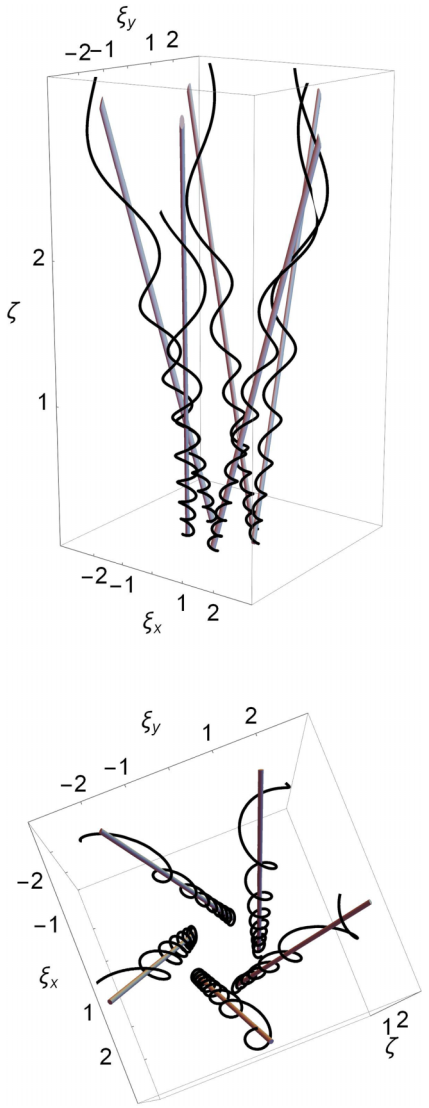

FIG. 9. Same as in Fig. 7, but for five particles and for the beam in Fig. 3.

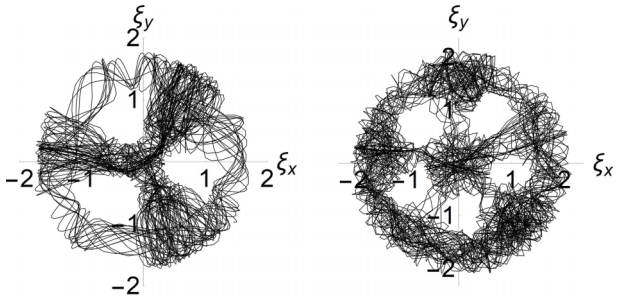

FIG. 10. The trajectories of the positive-polarizability particle placed in the beams with $n = 3$ and $n = 5$ projected onto the plane $\zeta = \text{const}$.

can result in jumping of particles between the tubes. The probability of such a phenomenon occurring was established numerically for complex knotted vortex lines [49].

As has already been mentioned, the drawings representing the computed particle trajectories should be viewed as illustrative only, prepared for γ of the order of 10^{-2}, chosen for clear visualization. A simple scaling argument leads to the conclusion that an identical effect will be achieved for smaller values of γ. However, in this case, the transported particles should be precisely placed in the potential valleys and strongly cooled (e.g., approximately microkelvin), which implies their slow motion and the necessity of determining the trajectories for a very long (from the point of view of the efficiency of numerical calculations) time.

It should also be noted that another parameter (β) remains at our disposal that can be used to rescale the radial size of the beam structures if needed.

As we know, if a particle with $\alpha > 0$ is inserted into a beam of this type, regions of low irradiance should exert a repulsive effect on it. As a result, characteristic holes ought to remain in the chaotic trajectory of such a particle, which cannot be penetrated. This situation is presented in Fig. 10 for $n = 3$ and $n = 5$ in the form of a projection of the calculated trajectories on the plane $\zeta = \text{const}$. A three-dimensional drawing would be unreadable for obvious reasons. In line with the previous discussion, to weaken the effect of the scattering force on the trajectory it was necessary to reduce the size of the spheres to 8 nm.

Figure 11 illustrates the trajectories of two particles: one with $\alpha < 0$ and the other with $\alpha > 0$ placed simultaneously in a beam with $n = 3$. As can be observed, the former moves inside the hole created by the trajectory of the latter.

Figure 11 highlights the extremely chaotic nature of the positively polarizable particle trajectories resulting from the eminently nonlinear form of the equations of motion in a very complex potential with many minima, maxima, and saddle points versus fairly regular trajectories of negatively polarizable particles (the potential inside low-irradiance tubes is quite smooth).

IV. CONCLUDING REMARKS

In conclusion, it should be stressed that the choice of a suitable Gaussian beam prefactor gives the possibility of designing beams that exhibit low-intensity tubes. In Sec. II,

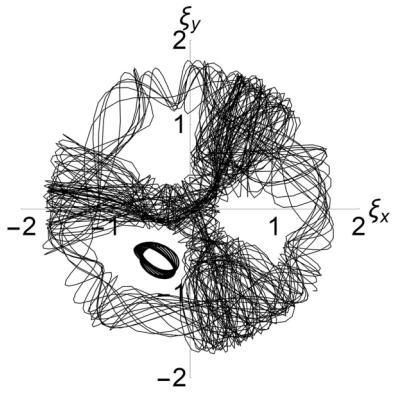

FIG. 11. The trajectories of two particles placed simultaneously in the beam in Fig. 1. The small trajectory corresponds to the particle of negative polarizability, and the large one corresponds to that of positive polarizability.

the prefactor was chosen in the form of a polynomial corresponding to the superposition of two Gaussian beams: a fundamental one and one that exhibits a vortex of the nth degree on the propagation axis. Due to the interference, this vortex gets split into n vortices located symmetrically on the circle, resulting in the appearance of the mentioned black wormholes. They can constitute independent lines for guiding particles. The results of the numerically performed calculations, presented in Sec. III, showed that particles with negative polarizability, neglecting some transverse oscillations, do indeed move along trajectories determined by lines of vanishing wave intensity. The influence of the scattering force on the motion was estimated in the case of dielectric nanospheres, and it was proved not to exert a significant effect on them.

Trajectories calculated for positively polarizable particles showed the opposite character: they have a very chaotic nature but avoid the mentioned areas. In this case, the scattering force should be accounted for since its impact on trajectories is significant.

Finally, it can be added that by choosing other polynomial prefactors, Gaussian beams can be obtained with various irradiance holes, designed as required. Figure 12 shows a transverse cross section of several Gaussian beams in which the areas of zero irradiance have been designed by choosing the appropriate polynomial prefactors.

The first two beams have hole distributions corresponding to the letters r and v from the Braille alphabet. They are

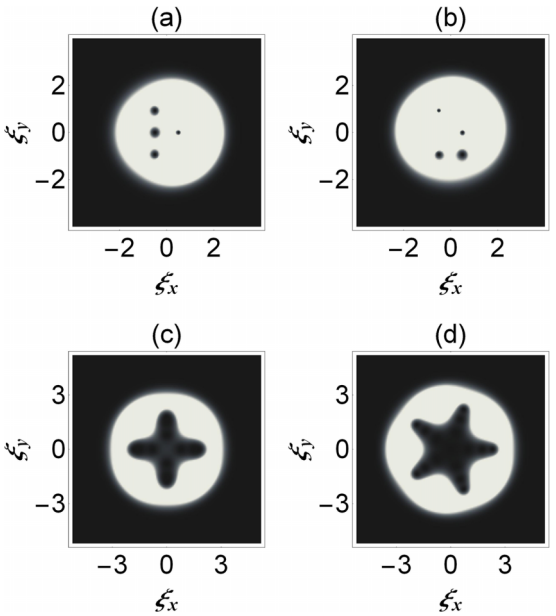

FIG. 12. Cross sections of the beams exhibiting some special patterns: (a) and (b) letters r and v of the Braille alphabet, (c) a cross, and (d) a star.

generated using the superposition of five Gaussian beams with vorticities of 0,1,2,3, and 4 (the parameter β is maintained below, which enables the pattern to be easily resized):

$$\tilde{\psi}_{(a)}(s) = [(\beta s + a)^2 + b^2][(\beta s)^2 - b^2], \tag{34a}$$

$$\tilde{\psi}_{(b)}(s) = [(\beta s + a)^2 + b^2](\beta s - a)(\beta s - a + ib), \tag{34b}$$

where a and b are certain real constants (fixed here to be $a = 0.75$ and $b = 1.4$).

In order to generate patterns representing a cross or a star, more components are needed. They can be obtained correspondingly with

$$\tilde{\psi}_{(c)}(s) = [(\beta s)^4 - 50][(\beta s)^4 - 25][(\beta s)^4 - 2], \tag{35a}$$

$$\tilde{\psi}_{(d)}(s) = [(\beta s)^5 - 500][(\beta s)^5 - 120][(\beta s)^5 - 6]\beta s. \tag{35b}$$

These are high-order polynomials, which means that high-vorticity beams are required to interfere. In the first case one needs four beams with vorticities of 0, 4, 8, and 12 with appropriate relative intensities, and in the second case one needs beams with vorticities of 1, 6, 11, and 16.

[1] A. E. Siegman, *Lasers* (University Science Books, Mill Valley, CA, 1986).
[2] M. Lax, W. H. Louisell, and W. B. McKnight, From Maxwell to paraxial wave optics, Phys. Rev. A **11**, 1365 (1975).
[3] H. Kogelnik and T. Li, Laser beams and resonators, Appl. Opt. **5**, 1550 (1966).
[4] L. W. Davis and G. Patsakos, TM and TE electromagnetic beams in free space, Opt. Lett. **6**, 22 (1981).
[5] S. Nemoto, Nonparaxial Gaussian beams, Appl. Opt. **29**, 1940 (1990).
[6] L. Mandel and E. Wolf, *Optical Coherence and Quantum Optics* (Cambridge University Press, New York, 1995).
[7] S. R. Seshadri, Electromagnetic Gaussian beam, J. Opt. Soc. Am. A **15**, 2712 (1998).
[8] G. Rodríguez-Morales and S. Chávez-Cerda, Exact nonparaxial beams of the scalar Helmholtz equation, Opt. Lett. **29**, 430 (2004).

[9] S. V. Ershkov and J. King, Exact solution of Helmholtz equation for the case of non-paraxial Gaussian beams, J. King Saud Univ. Sci. **27**, 198 (2015).

[10] M. V. Selina, Nonparaxial Gaussian beam, J. Opt. **49**, 338 (2020).

[11] B. E. A. Saleh and M. C. Teich, *Fundamentals of Photonics* (Wiley-Interscience, New York 2007).

[12] A. Ashkin, J. M. Dziedzic, J. E. Bjorkholm and S. Chu, Observation of a single-beam gradient force optical trap for dielectric particles, Opt. Lett. **11**, 288 (1986).

[13] S. Chu, J. E. Bjorkholm, A. Ashkin and A. Cable, Experimental observation of optically trapped atoms, Phys. Rev. Lett. **57**, 314 (1986).

[14] J. D. Miller, R. A. Cline, and D. J. Heinzen, Far-off-resonance optical trapping of atoms, Phys. Rev. A **47**, R4567(R) (1993).

[15] *Optical Tweezers: Methods and Applications*, edited by M. Padgett, J. Molloy, and D. McGloin, Series in Optics and Optoelectronics (CRC Press, Boca Raton, FL, 2010).

[16] J. Yin, Y. Zhu, W. Jhe, and Z. Wang, Atom guiding and cooling in a dark hollow laser beam, Phys. Rev. A **58**, 509 (1998).

[17] J. Yin, Y. Zhu, W. Wang, Y. Wang, and W. Jhe, Optical potential for atom guidance in a dark hollow laser beam, J. Opt. Soc. Am. B **15**, 25 (1998); Optical potential for atom guidance in a dark hollow laser beam: Errata, *ibid.* **15**, 1816 (1998).

[18] X. Xu, Y. Wang, and W. Jhe, Theory of atom guidance in a hollow laser beam: Dressed-atom approach, J. Opt. Soc. Am. B **17**, 1039 (2000).

[19] I. Białynicki-Birula, Z. Białynicka-Birula, and N. Drozd, Trapping of charged particles by Bessel beams, in *The Angular Momentum of Light*, edited by D. L. Andrews and M. Babiker (Cambridge University Press, Cambridge, 2012), p. 280.

[20] D. Barredo, V. Lienhard, P. Scholl, S. de Léséleuc, T. Boulier, A. Browaeys, and T. Lahaye, Three-dimensional trapping of individual Rydberg atoms in ponderomotive bottle beam traps, Phys. Rev. Lett. **124**, 023201 (2020).

[21] F. Almeida, I. Sousa, O. Kremer, B. P. da Silva, D. S. Tasca, A. Z. Khoury, G. Temporão, and T. Guerreiro, Trapping microparticles in a structured dark focus, Phys. Rev. Lett. **131**, 163601 (2023).

[22] B. Melo, I. Brandão, B. S. P. da, R. B. Rodrigues, A. Z. Khoury, and T. Guerreiro, Optical trapping in a dark focus, Phys. Rev. Appl. **14**, 034069 (2020).

[23] V. I. Balykin and V. S. Letokhov, The possibility of deep laser focusing of an atomic beam into the Å-region, Opt. Commun. **64**, 151 (1987).

[24] X. Xu, V. G. Minogin, K. Lee, Y. Wang, and W. Jhe, Guiding cold atoms in a hollow laser beam, Phys. Rev. A **60**, 4796 (1999).

[25] J. Yin, W. Gao, and Y. Zhu, Generation of dark hollow beams and their applications, Prog. Opt. **45**, 119 (2003).

[26] Y. Cai and S. He, Propagation of various dark hollow beams in a turbulent atmosphere, Opt. Express **14**, 1353 (2006).

[27] F. Khannous, M. Boustimi, H. Nebdi, and A. Belafhal, Theoretical investigation on the hollow Gaussian beams propagating in atmospheric turbulent, Chin. J. Phys. **54**, 194 (2016).

[28] F. Gori, G. Guattari, and C. Padovani, Bessel-Gauss beams, Opt. Commun. **64**, 491 (1987).

[29] A. April, Bessel–Gauss beams as rigorous solutions of the Helmholtz equation, J. Opt. Soc. Am. A **28**, 2100 (2011).

[30] J. Mendoza-Hernández, M. L. Arroyo-Carrasco, M. D. Iturbe-Castillo, and S. Chávez-Cerda, Laguerre–Gauss beams versus Bessel beams showdown: Peer comparison, Opt. Lett. **40**, 3739 (2015).

[31] L. Allen, M. W. Beijersbergen, R. J. C. Spreeuw, and J. P. Woerdman, Orbital angular momentum of light and the transformation of Laguerre-Gaussian laser modes, Phys. Rev. A **45**, 8185 (1992).

[32] A. April, Nonparaxial elegant Laguerre–Gaussian beams, Opt. Lett. **33**, 1392 (2008).

[33] W. Nasalski, Elegant Laguerre–Gaussian beams – Formulation of exact vector solution, J. Opt. **20**, 105601 (2018).

[34] T. Radożycki, Properties of special hyperbolic Bessel-Gaussian optical beams, Phys. Rev. A **104**, 023520 (2021).

[35] T. Kuga, Y. Torii, N. Shiokawa, T. Hirano, Y. Shimizu, and H. Sasada, Novel optical trap of atoms with a doughnut beam, Phys. Rev. Lett. **78**, 4713 (1997).

[36] M. Yan, J. Yin, and Y. Zhu, Dark-hollow-beam guiding and splitting of a low-velocity atomic beam, J. Opt. Soc. Am. B **17**, 1817 (2000).

[37] Q. Sun, K. Zhou, G. Fang, G. Zhang, Z. Liu, and S. Liu, Hollow sinh-Gaussian beams and their paraxial properties, Opt. Express **20**, 9682 (2012).

[38] G. Indebetouw, Optical vortices and their propagation, J. Mod. Opt. **40**, 73 (1993).

[39] I. V. Basistiy, V. Yu. Bazhenov, M. S. Soskin, and M. V. Vasnetsov, Optics of light beams with screw dislocations, Opt. Commun. **103**, 422 (1993).

[40] D. Rozas, C. T. Law, and G. A. Swartzlander, Jr., Propagation dynamics of optical vortices, J. Opt. Soc. Am. B **14**, 3054 (1997).

[41] A. A. Kovalev, V. V. Kotlyar, and A. P. Porfirev, Orbital angular momentum and topological charge of a multi-vortex Gaussian beam, J. Opt. Soc. Am. A **37**, 1740 (2020).

[42] D. J. Stevenson, F. J. Gunn-Moore, and K. Dholakia, Light forces the pace: Optical manipulation for biophotonics, J. Biomed. Opt. **15**, 041503 (2010).

[43] F. M. Fazal and S. M. Block, Nat. Photonics **5**, 318 (2011).

[44] M. Woerdemann, *Structured Light Fields: Applications in Optical Trapping, Manipulation, and Organisation* (Springer, Berlin, 2012).

[45] R. W. Bowman and M. J. Padgett, Optical trapping and binding, Rep. Prog. Phys. **76**, 026401 (2013).

[46] D. G. Grier, A revolution in optical manipulation, Nature (London) **424**, 810 (2003).

[47] D. S. Bradshaw and D. L. Andrews, Manipulating particles with light: Radiation and gradient forces, Eur. J. Phys. **38**, 034008 (2017).

[48] Y. Liang, S. Yan, B. Yao, and M. Lei, Direct observation and characterization of optical guiding of microparticles by tightly focused non-diffracting beams, Opt. Express **27**, 37975 (2019).

[49] T. Radożycki, Knotted trajectories of neutral and charged particles in Gaussian light beams, Phys. Rev. A **102**, 063101 (2020).

[50] D. Xu, Z. Mo, J. Jiang, H. Huang, Q. Wei, Y. Wu, X. Wang, Z. Liang, H. Yang, H. Chen, H. Huang, H. Liu, D. Deng,

and L. Shui, Guiding particles along arbitrary trajectories by circular Pearcey-like vortex beams, Phys. Rev. A **106**, 013509 (2022).

[51] E. Abramochkin and V. Volostnikov, Spiral-type beams: Optical and quantum aspects, Opt. Commun. **125**, 302 (1996).

[52] M. V. Berry, A note on superoscillations associated with Bessel beams, J. Opt. **15**, 044006 (2013).

[53] T. Radożycki, Few-parameter noncylindrical paraxial optical beam described by the modified Bessel function, Phys. Rev. A **106**, 053510 (2022).

[54] N. B. Delone and V. P. Krainov, AC Stark shift of atomic energy levels, Phys.-Usp. **42**, 669 (1999).

[55] R. Grimm, M. Weidemüller, and Y. B. Ovchinnikov, Optical dipole traps for neutral atoms, Adv. Atom. Mol. Opt. Phys. **42**, 95 (2000).

[56] M. Kerker, *The Scattering of Light and Other Electromagnetic Radiation* (Academic, New York, 1969).

[57] Y. Harada and T. Asakura, Radiation forces on a dielectric sphere in the Rayleigh scattering regime, Opt. Commun. **124**, 529 (1996).

[58] T. Radożycki, Guiding neutral particles endowed with a magnetic moment by an electromagnetic wave carrying orbital angular momentum: Quantum mechanics, Phys. Rev. A **98**, 013424 (2018).